6-2023

Impacts of a Cascadia Subduction Zone Earthquake on Water Levels and Wetlands of the Lower Columbia River and Estuary

M. W. Brand
Pacific Northwest National Laboratory

Heida Diefenderfer
Pacific Northwest National Laboratory

J. E. O'Connor
U.S. Geological Survey, Portland

Amy B. Borde
Pacific Northwest National Laboratory

D. A. Jay
Portland State University

See next page for additional authors

Citation Details

Brand, M. W., Diefenderfer, H. L., O'Connor, J. E., Borde, A. B., Jay, D. A., Al-Bahadily, A., ... & Talke, S. A. (2023). Impacts of a Cascadia subduction zone earthquake on water levels and wetlands of the lower Columbia River and estuary. Geophysical Research Letters, 50(14), e2023GL103017.

Geophysical Research Letters

RESEARCH LETTER
10.1029/2023GL103017

Key Points:

- Earthquake-induced subsidence results in the movement of ~93% of intertidal habitat to lower habitat zones
- Post earthquake, tidal range increases by up to 0.25 m in channels; capturing such changes requires a dynamic model
- Both subsidence and changes in tidal range alter habitats, especially sandflats and low marshes

Supporting Information:

Supporting Information may be found in the online version of this article.

Correspondence to:

M. W. Brand,
matthew.brand@pnnl.gov

Citation:

Brand, M. W., Diefenderfer, H. L., O'Connor, J. E., Borde, A. B., Jay, D. A., Al-Bahadily, A., et al. (2023). Impacts of a Cascadia subduction zone earthquake on water levels and wetlands of the lower Columbia River and estuary. *Geophysical Research Letters*, *50*, e2023GL103017. https://doi.org/10.1029/2023GL103017

Received 27 JAN 2023
Accepted 14 JUN 2023

Impacts of a Cascadia Subduction Zone Earthquake on Water Levels and Wetlands of the Lower Columbia River and Estuary

M. W. Brand[1,2], H. L. Diefenderfer[1,3], J. E. O'Connor[4], A. B. Borde[1], D. A. Jay[5], A. Al-Bahadily[6], M. McKeon[1], and S. A. Talke[7]

[1]Pacific Northwest National Laboratory, Coastal Sciences Division, Sequim, WA, USA, [2]University of California, Irvine, Irvine, CA, USA, [3]University of Washington, Seattle, WA, USA, [4]U.S. Geological Survey, Portland, OR, USA, [5]Portland State University, Portland, OR, USA, [6]Mustansiriyah University, Baghdad, Iraq, [7]California Polytechnic State University, San Luis Obisbo, CA, USA

Abstract Subsidence after a subduction zone earthquake can cause major changes in estuarine bathymetry. Here, we quantify the impacts of earthquake-induced subsidence on hydrodynamics and habitat distributions in a major system, the lower Columbia River Estuary, using a hydrodynamic and habitat model. Model results indicate that coseismic subsidence increases tidal range, with the smallest changes at the coast and a maximum increase of ~10% in a region of topographic convergence. All modeled scenarios reduce intertidal habitat by 24%–25% and shifts ~93% of estuarine wetlands to lower-elevation habitat bands. Incorporating dynamic effects of tidal change from subsidence yields higher estimates of remaining habitat by multiples of 0–3.7, dependent on the habitat type. The persistent tidal change and chronic habitat disturbance after an earthquake poses strong challenges for estuarine management and wetland restoration planning, particularly when coupled with future sea-level rise effects.

Plain Language Summary The land in many estuaries along the Pacific Rim has been repeatedly changed by major earthquakes. Previous earthquakes, such as the CE 1700 rupture along the 1,000-km Cascadia Subduction Zone of western North America, produced as much as 2 m of land-surface lowering. This study employs a hydrodynamic model to show that the relative sea-level rise resulting from such lowering would increase tidal range and affect nearly all existing wetland habitat in the lower Columbia River Estuary. In our primary scenario, approximately ~93% of current wetland habitat converts to lower-elevation types, with changes largely due to land-surface lowering but also influenced by tidal changes. Thus, the chronic, long-term disturbance to habitat conditions after an earthquake poses a similar long-term risk to estuarine ecology as extreme global sea-level rise scenarios. Understanding such earthquake effects may assist the development of more resilient habitat restoration strategies.

1. Introduction

Large megathrust earthquakes on the Cascadia Subduction Zone (CSZ) have repeatedly caused episodes of tsunami inundation, coseismic tectonic subsidence, and relative sea-level rise along the Eastern Pacific coastline between British Columbia, Canada, and northern California (Atwater, 1987; Atwater & Yamaguchi, 1991). Though the immediate hazards posed to humans by future tsunami inundation have been characterized (Chen et al., 2021; Kalmbacher & Hill, 2015; Tolkova et al., 2015; Yeh et al., 2012), the potentially persistent hydrodynamic and ecologic effects of coseismic coastal subsidence are less studied, but may be substantial. The most recent CSZ rupture in CE 1700 produced up to 2 m of coseismic subsidence, and caused an instantaneous conversion of spruce-forested tidal marshes and wetlands to tidal flats throughout the Pacific Northwest (Atwater et al., 2011; Nelson et al., 1995; Yamaguchi et al., 1997). Earthquake-induced topographic changes can feed back into tidal and circulation patterns; for example, the M_2 tidal constituent in Anchorage, Alaska, decreased by ~0.2 m (~5%) in response to vertical land motion caused by the 1964 Great Alaskan Earthquake (Talke & Jay, 2020). Topographic and hydrodynamic changes may also strongly affect estuarine ecologic systems and large, ongoing programs focused on restoring tidal river wetlands and estuarine salmon habitat (Baldwin et al., 2019; Gerwing et al., 2020).

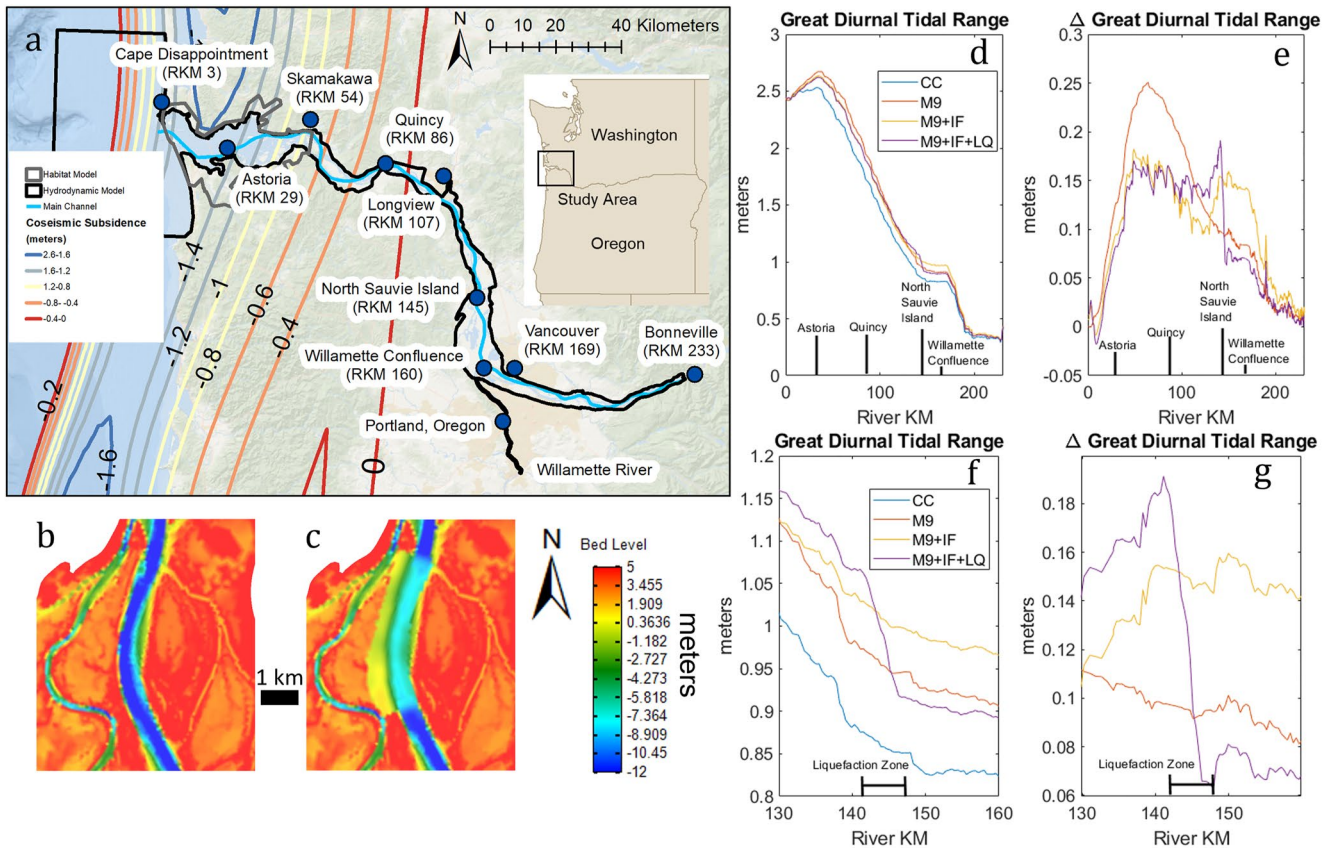

Figure 1. (a) Location of the lower Columbia River Estuary (LCRE) and predicted co-seismic land surface elevation change as contour elevations predicted by Madin and Burns (2012) with points of interest; (b) current topography and bathymetry at North Sauvie Island near RKM-145, (c) modified topography at RKM-145 resulting from 3 m of liquefaction induced subsidence and an average 6 m reduction in channel depth caused by east-directed lateral spreading of 500 ha of floodplain, (d) Greater Diurnal Tidal Range (GT) from the mouth to the head of tides for current conditions (CC) and the 3 post-event scenarios (see Section 2.2) (e) Change in GT relative to CC resulting from the M9, M9+IF, and M9+IF+LQ scenarios (e) zoom in on liquefaction zone for GT (f) and change in GT (g) for all scenarios.

In this study, we investigate the potential effects of a M9 subduction zone earthquake on tidal datums and wetland habitats within the lower Columbia River Estuary (LCRE; Figure 1). Located close to the offshore subduction zone, the seaward portions of the estuary are undergoing interseismic uplift and a corresponding drop in relative sea-level (Burgette et al., 2009; Talke et al., 2020). This buffer against sea-level rise effects will be altered during an M9 event; predictions indicate the land surface could drop up to 1.4–1.6 m at the coast (Madin & Burns, 2012, Figure 1). A sharp decrease in subsidence occurs landward, and only about ~0.3 m of subsidence would occur at river kilometer (RKM) 86. A M9 could also destroy levees and other coastal infrastructure, for example, through liquefaction or erosion (Nasseri et al., 2014; Takabatake et al., 2019). Hydrodynamic changes will likely occur, because tides, circulation, and salinity intrusion in the LCRE are sensitive to bathymetric change (Al-Bahadily, 2020; Helaire et al., 2019). In these respects, the LCRE is representative of the types of changes that may occur in other PNW estuaries as a result of rapid bathymetric change (see, e.g., Eidam et al., 2021).

To investigate the estuarine response to an M9 event in the LCRE, we develop a numerical model and evaluate how tidal datums and their spatial boundaries may shift in response to the predicted coseismic topographic changes. Because different estuary species and wetland types occur within specific tidal elevation bands, we are able to estimate changes in spatial patterns of habitat disturbance. Additionally, we determine whether habitat change is driven by subsidence only, or whether the feedback of altered bathymetry on the tides influences the ecological disturbance. The near total modification in ecological habitat that our model predicts for a co-seismic event poses challenges to the long-term viability of wetlands and wetland restoration projects. This event causes relative sea-level rise (rSLR) on-par with future high-emissions sea-level rise scenarios, but on a much shorter time scale than anthropogenic sea-level rise (SLR).

2. Methods

2.1. Study Area

The Columbia River flows 2,000 km from its headwaters in British Columbia, Canada, to its confluence with the northeast Pacific Ocean (Figure 1). It flows through a rising coastal subduction zone with relatively steep along-channel and lateral topography (O'Connor et al., 2021). Mean annual flow at the estuary mouth is ~7,350 $m^3\ s^{-1}$ and typically ranges between about 1,800 and 16,000 $m^3\ s^{-1}$ (Jay & Naik, 2011). The tides propagate 244 km from the ocean to Bonneville Dam, the head of tides. Tides are mesotidal and mixed semidiurnal, with a mean tidal range of 2.06 m at Astoria, Tongue Point (RKM-29; Figure 1), and a great diurnal tidal range (GT) of 2.62 m (Talke et al., 2020). Tides are amplified in the lower estuary, and dissipate upstream due to friction and interaction with Columbia and Willamette River inputs. Dredging, diking, inlet modification and other anthropogenic modifications have amplified tidal ranges in the reach between Astoria (RKM-25) and Quincy (RKM-86) by ~5–20% (Helaire et al., 2019; Talke et al., 2020). Anthropogenic tidal changes have propagated as far upsteam as the Portland metropolitan area (Helaire et al., 2019).

The LCRE hosts diverse ecosystems such as tidal marsh wetlands and spruce swamps, and is an important rearing and migratory corridor for several anadromous fishes, including Pacific salmon, steelhead, and Pacific lamprey (Naiman et al., 2012). By 1980, approximately 70% of the historical wetland area of ~146,800 ha was lost to reclamation (Marcoe & Pilson, 2017). Between 2004 and 2021, 77 restoration projects added ~2,830 ha of floodplain habitat (Littles et al., 2022). The effect of a CSZ event on remnant and restored habitat is currently unknown, and not considered in planning.

2.2. Scenarios

We employ four scenarios to investigate the effects of extreme, but plausible, changes to system bathymetry and infrastructure. The scenarios simulate current conditions (CC), M9 subsidence (M9), M9 subsidence plus infrastructure failure (M9+IF), and a coupled M9+IF scenario with liquefaction and lateral spreading of the floodplain at RKM-145 (M9+IF+LQ). The model incorporates all significant flow control infrastructure within the LCRE: pile dikes, flood-control levees, and jetties (details located in Text S1 in Supporting Information S1). All our M9 scenarios use the tectonic coseismic land-level changes predicted by Madin and Burns (2012) for a M9 CSZ earthquake similar to the CE 1700 CSZ rupture (Figure 1a). This scenario, while extreme, represents a plausible impact resulting from a CSZ rupture. Though possible that smaller subsidence events could occur, these were not modeled. The infrastructure failure (M9+IF) scenario assumes that all flood and navigational infrastructure, including jetties, pile dikes, and flood-control levees, are destroyed or compromised such that they exert no hydrodynamic influence. The liquefaction scenario explores the possible influence of seismically triggered mass movement, based on a possible past example (see Text S5 in Supporting Information S1). For the M9+IF+LQ scenario, we postulate lateral spreading of a 500 ha area of floodplain into the main channel along Sauvie Island (RKM-145), thereby locally reducing floodplain elevations and increasing local channel elevation (Figure 1c). This scenario is consistent with geologic evidence of previous liquefaction (Text S5 in Supporting Information S1) and could significantly impact local circulation; however, the far field effects are presently unknown.

2.3. Hydrodynamic Model

Hydrodynamic simulations were conducted with the Delft3D-Flexible Mesh model, widely applied to estuarine hydrodynamics (Nederhoff et al., 2021; Symonds et al., 2016). Details on model setup, calibration, and evaluation are in Text S1–S4 in Supporting Information S1, including calibration results and comparison to previously published studies. The domain extends from Bonneville Dam to the continental shelf. Following Nederhoff et al. (2021) and Helaire et al. (2019), a depth-integrated 2D mode was used; because we focus on water levels and wetlands, we do not consider the hydrodynamic effects of salinity intrusion and density stratification (see also Helaire et al., 2019). Most present LCRE wetlands landward of RKM-20 contain freshwater or oligohaline vegetation (Borde et al., 2020), validating this assumption. The model grid resolution varied from 1 km offshore to 100 m within the estuary and tidal river. The time period modeled was January 2017 through April 2020 (peak freshet flow in May 2018 = 14,000 m^3/s), with riverine discharge imposed at Bonneville Dam and the Willamette, Cowlitz, Lewis, and Sandy Rivers.

Our hydrodynamic change analysis focused on evaluating the tidally dominated floodplain of the lowermost 54 km, the region most influenced by co-seismic subsidence. Water level data were reported in 15 min time

increments, both on a 500 × 500 m grid within the estuary and approximately every 800 m along the main channel centerline in the estuary and tidal river (blue line in Figure 1a). These outputs were evaluated to estimate tidal datums and the Great Diurnal Range (GT), defined as "The difference in height between mean higher high water (MHHW) and mean lower low water (MLLW)" (National Atmospheric and Oceanic Administration (NOAA) 2022). We calculated the changes to GT during the low-flow period, defined as July through October, to minimize the effects of fluvial inputs.

2.4. Habitat Modeling

Changes in tidal datums for the habitat model after an M9 event are estimated by first differencing tidal statistics (such as mean-high water) between the baseline 2018 CC scenario and the three M9 scenarios. This offset was then applied to the NOAA datums. This approach accounts for differences in sea-level and tides between our 2017–2020 simulations and the 1983–2001 epoch used to evaluate NOAA datums (Text S3 in Supporting Information S1 contains further details). Results between tidal gauges were linearly interpolated between NOAA stations (Cape Disappointment, Astoria, and Skamokawa) using the polygons in Figure S12 in Supporting Information S1.

Using the National Land Cover Database (NLCD) (2019) data set and habitat information from Borde et al. (2020), we map multiple habitat types (forested, shrub, high marshland, low marshland, sandflat, and subtital habit) to elevational bands. The vertical zonation corresponds well to tidal datums defined by the National Oceanic and Atmospheric Administration (NOAA, 2022) at Cape Disappointment, Astoria, and Skamokawa. For example, the boundary between low marsh and high marsh at Cape Disappointment is 2.17 m (above NAVD88), which corresponds to the MHW level. Thus, estuarine habitats are strongly tied to the frequency and duration of inundation, which are influenced by land-surface elevation, tidal dynamics, and river flow. The wetland boundary to habitat type mapping was validated against NLCD (2019) habitat classifications and showed "very good" agreement using the Kappa statistic (Text S4 in Supporting Information S1; Monserud & Leemans, 1992).

3. Changes to Tidal Hydrodynamics

Coseismic subsidence from an M9 event affects great diurnal range (GT) in a spatially variable way (Figure 2). Along the main channel, GT changes are small near the ocean boundary (<0.1 m) but increase to 0.25 m in the eastern portion of the estuary for RKM-41-54, near the point of estuarine convergence at Skamokawa/Welch Island (Figure 2c/d). A likely cause is the decreased damping caused by smaller tidal currents and lower friction in the deepened channel. Helaire et al. (2019) found large increases in the M_2 tide in the same reach as a consequence of historical channel deepening. The greatest changes in GT, up to 1.0 m, are modeled for tidal flats and wetlands that previously were partially inundated (so that they were bare at low water) (Figure 2a/b). Thus, the patchy pattern of large tidal change indicates locations that are more frequently or even continuously inundated after an M9 event.

Adding infrastructure failure to coseismic subsidence (M9+IF, Figure 2b) reduces GDTR amplification in the lower estuary compared to the M9 (Figure 2a) scenario. This owes primarily to floodplain levee removal, thereby opening large floodplain areas for inundation, transport and storage. The maximum effect of infrastructure failure occurs at RKM 50–100, where GDTR amplication diminishes by ∼0.08 m (compared to M9 alone), about a third of the total M9 effect (Figure 1d/e). The M9+IF+LQ scenario showed little difference in spatial change of GDTR compared to M9+IF for the lower estuary up to RKM-∼80 (Figure S4 in Supporting Information S1), but large differences near the liquefaction zone (Figure 1f/g).

Increased tidal range from coseismic subsidence extends well into the Tidal River Reach (as defined by Jay et al., 2016) to the confluence of the Willamette and Columbia River (RKM-160; Figure 1d/e). The M9 scenario produces larger tidal ranges than the M9+IF scenario between RKM 0–130. Farther upstream, the M9+IF scenario produces tidal range change of up to ∼0.15 m, ∼0.05 m greater than the M9 scenario (Figure 1e). The increased influence of infrastructure failure is a result of the simulated loss of pile dikes upstream of Longview (RKM-107, Figure 1). These pile dikes constrict the main part of the channel, reducing its cross-sectional area and increasing channel velocities under present-day flow conditions. Their removal under the M9+IF scenario decreases frictional effects, thereby lowering MWL and MLLW stages but not significantly affecting MHHW levels. A similar effect occurred historically by streamlining and deepening of the navigation channel (Jay & Naik, 2011; Jay et al., 2015; Helaire et al., 2019).

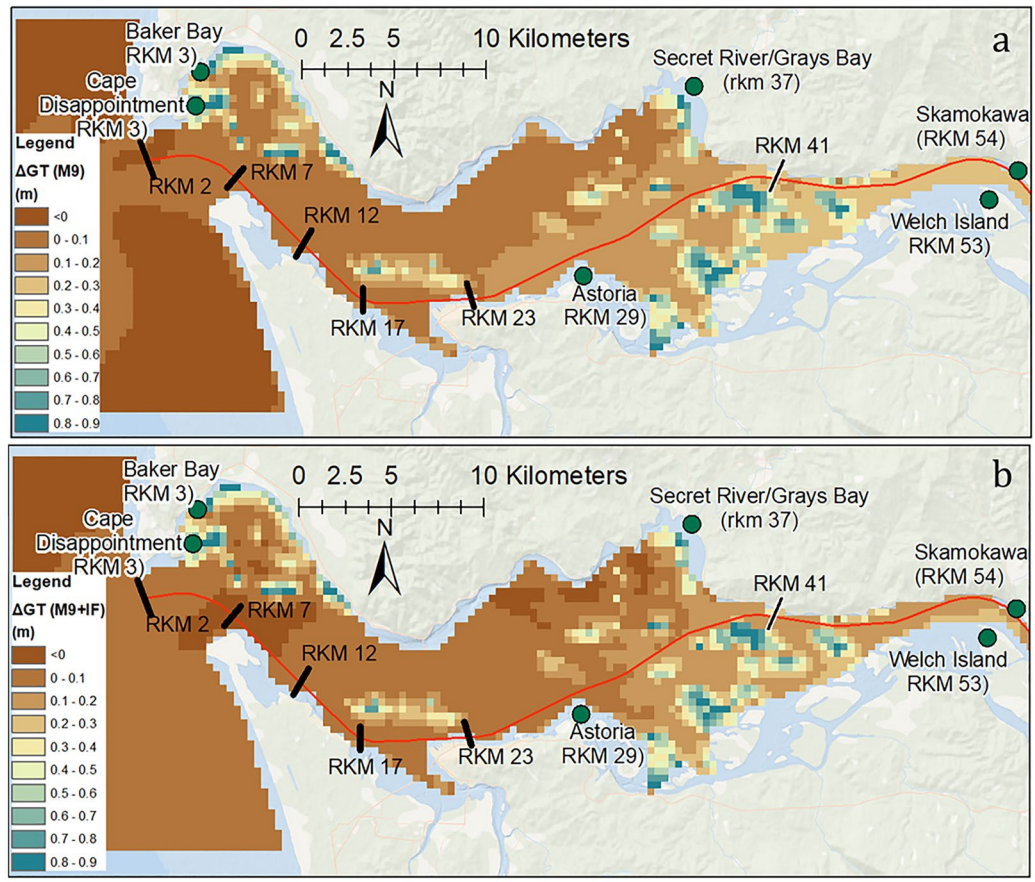

Figure 2. Changes in tidal range within (a) the lower estuary for the M9 and (b) M9+IF scenarios.

For the liquefaction scenario (M9+IF+LQ), the hydrodynamic model predicts amplication (by as much 0.18 m) of the tidal wave downstream of the liquefaction site due to partial reflection from the partly filled and constricted main channel (Figure 1f/g). Upstream of the liquefaction site, the tidal wave is attenuated and the change in tidal range is less than for the M9+IF scenario. The M9+IF+LQ reflection effect is greatest near the liquefaction site at RKM-141 and diminishes downstream, becoming undetectable around RKM-90 (Figure 1d). Thus, geomorphic processes as well as tectonic deformation and infrastructure failure can alter tidal hydrodynamics. Similar liquefaction might occur at multiple locations in the LCRE; thus, the M9+IF+LQ scenario is indicative, but not definitive.

4. Changes to Estuarine Habitats

4.1. Habitat Model Results

After a M9 CSZ rupture, model results suggest that subtidal and intertidal areas in the estuary will increase by 2,600 ha from ~49,100 to ~51,800 ha, resulting from the conversion of upland to intertidal or subtidal habitat (Figure 3, Table 1). A large increase of subtidal habitat occurs, ~7,500 ha, along with about net 4,900 ha decrease in intertidal habitat (Table 1). The squeeze in intertidal habitat is caused by LCRE hypsometry, which is marked by steep uplands, except in urbanized regions and west of RKM-20. The habitat conversion matrix (Table 1) shows how much of each habitat type under current conditions (each row of column 1) is converted to a different habitat type post-CSZ event (columns labeled SUB to UP). For example, the model predicts all existing low marsh (LM; row 3) will convert to subtidal (SUB; 26.1%) or sandflat (FL; 72.8%) habitat (Table 1).

Our model predicts that all forested and shrub wetland estuarine habitats transform to a lower-elevation wetland classification. In all scenarios, only sandflat (4.81%) and high marsh (2.32%) intertidal bands retain some small portion of their original habitat (diagonal in the Habitat Conversion Matrix of Table 1). The (M9+IF) and

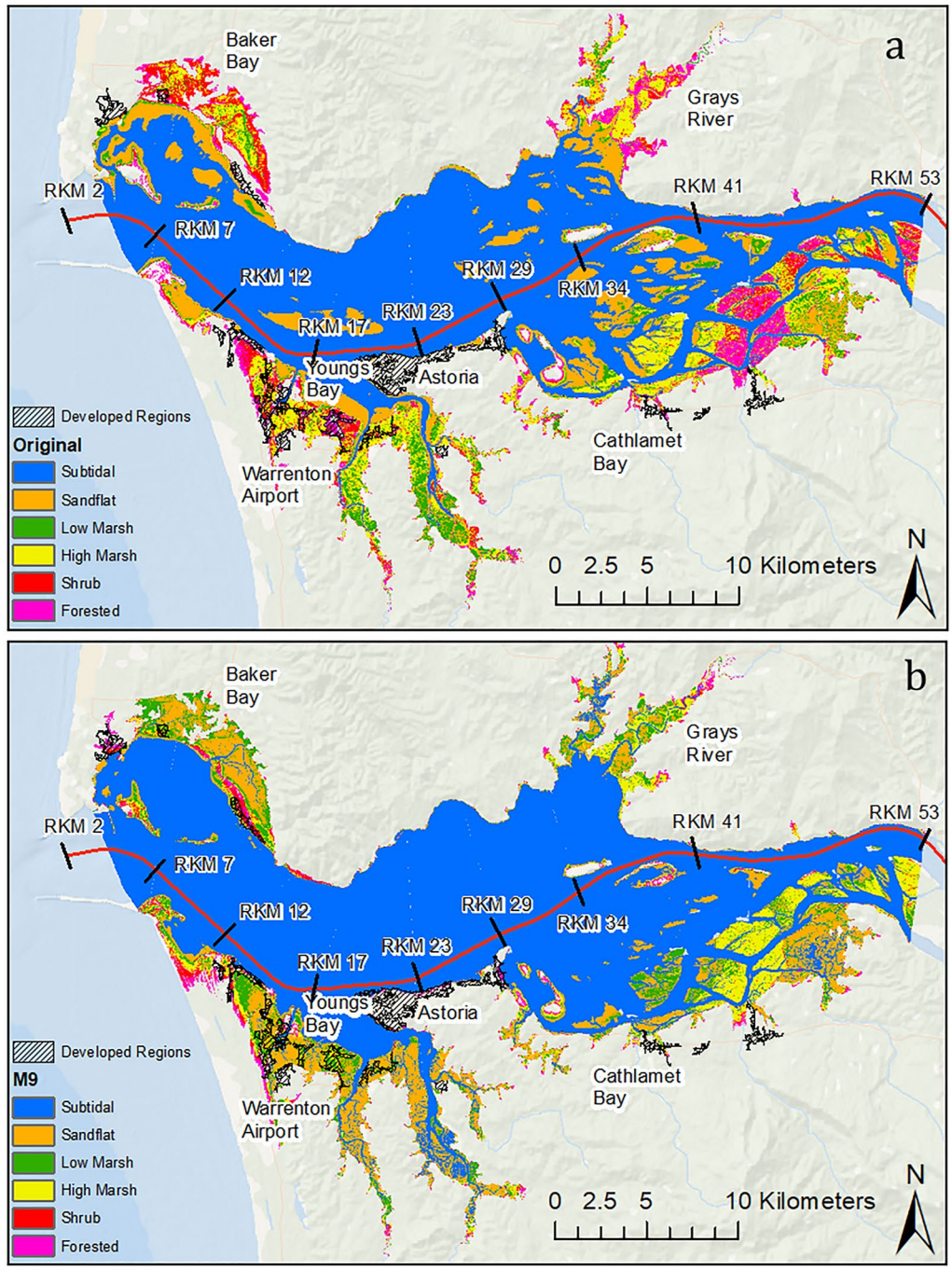

Figure 3. Present day (a) and Cascadia Subduction Zone (CSZ) rupture M9 scenario (b) habitat distributions.

(M9+IF+LQ) scenarios result in slightly lower predictions (2.0% and 4.6%, respectively) of sandflat preservation and little differences in the upper habitat communities. This result stems from the finding that changes to GDTR are driven by lower tidal low-waters.

The model also predicts considerable redistribution of possible habitat types. Overall, potential subtidal and low marsh habitats expand markedly, by 26% and 23%, respectively (these are elevation bands in which this habitat could develop). This expansion occurs at the expense of sandflats, high marsh, shrub, and forested wetlands, which show overall losses in potential area of 4%, 33%, 67%, and 64%, respectively (Table 1). Most of the conversion from high marsh and higher elevation habitats to sandflat habitat is in Baker Bay and Youngs Bay (Figure 3),

Table 1
Changes to CC (Current Conditions) to Land-Cover Proportions by Wetland Habitat Class (SUB = Subtidal, FL = Sandflats, LM = Low Marsh, HM = High Marsh, SH = Shrub/Scrub, FOR = Forested, UP = Upland) Predicted by Elevation and Tidal Inundation Metrics for Post-CSZ M9 Rupture Scenario

	Habitat area (hectares)		Habitat conversion matrix—M9 (bathtub model in paratheses)						
Habitat type	CC	M9	SUB	FL	LM	HM	SH	FOR	UP
Subtidal (SUB)	28,900	36,400	**100% (100%)**						
Sandflat (FL)	7,130	6,800	95.2% (98.7%)	**4.81% (1.33%)**					
Low Marsh (LM)	2,630	3,220	26.1% (38.3%)	72.8% (61.6%)	**0.00% (0.00%)**				
High Marsh (HM)	5,240	3,510	0.00% (0.550%)	75.4% (80.7%)	22.3% (17.7%)	**2.32% (1.12%)**			
Shrub (SH)	2,480	814	0.00% (0.00%)	25.8% (28.2%)	47.4% (47.8%)	26.8% (24.0%)	**0.00% (0.00%)**		
Forested (FOR)	2,760	999	0.00% (0.00%)	0.00% (0.00%)	29.8% (31.1%)	68.1% (66.6%)	1.99% (2.17%)	**0.00% (0.140%)**	
Upland (UP)	24,800	22,100	0.00% (0.00%)	0.00% (0.00%)	0.20% (0.190%)	3.40% (3.33%)	3.06% (3.08%)	3.99% (3.89%)	**89.4% (89.5%)**
All Habitat Sum	73,900	73,900							
Intertidal Habitat Sum	20,200	15,400							

Note. Percentage of habitat remaining its original class is shown in the emboldened diagonal of the cross tabulation matrix. Changes predicted by the bathtub model are shown in paratheses, and tables for M9+IF and M9+IF+LQ are in Tables S1 and S2 in Supporting Information S1.

mainly because these regions are expected to experience the largest coseismic subsidence (~1.4–1.6 m, Figure 1a). Regions farther east such as Cathlamet Bay and Grays River have less subsidence (~0.8–1.2 m) and therefore less drastic habitat transformations; there, forested and shrubland areas are converted to either high or low marsh (Figure 3).

We assess the aggregate influence of altered tides on habitat disturbance by recalculating results under the assumption of no tidal change; that is, using a "bathtub" model in which topographic elevations are lowered, but water levels remain the same relative to datums. Such an approach does not require hydrodynamic modeling, provides an "order of magnitude" assessment (see Table 1), but misses important "dynamic" changes resulting from altered tides, especially in the subtidal to low marsh habitat bands (Table 1). The effect of tidal change is most prominent in the easternmost section of the domain (RKM 41–53), where subsidence is smaller and tidal changes are larger, and in habitats that presently exhibit smaller GT. For example, the dynamic model predicts that 68.1% of sandflats in the easternmost region convert to subtidal conditions, while the bathtub predicts 91.3% (Table S3 and S4 in Supporting Information S1). However, dynamic model effects are reduced in the higher elevational intertidal habitat elevation bands. For example, the dynamic model predicts 94.7% of forest will convert to high marsh in the M9 scenario, with the bathub model predicting 94.1% conversion in the easternmost region. This result is consistent with the hydrodynamic model results demonstrating the majority of amplification is a result of lower MLLW.

4.2. Hydrodynamic and Habitat Modeling Uncertainties

The changes to tidal datums and habitat presented here are plausible, but exploratory results meant to assess the possible order-of-magnitude changes that may occur during the next CSZ rupture. The timing, magnitude, and extent of the next CSZ rupture are unknown and remain major sources of uncertainty, and the timing of an M9 event relative to sea-level rise may influence the tidal response and the habitat disturbance. The M9 scenarios adopted here provide a plausible set of scenarios using the median estimates of co-siesmic subsidence from Madin and Burns (2012), but is not definitive.

The M9+IF scenario used in this study represents an "end member" scenario and provides insights into the possible water level and tidal impacts of infrastructure failure. Other types of infrastructure failure also merit consideration, including bridge and dam failure. Similarly, the liquefaction scenario (M9+IF+LQ) is plausible and identifies possible (local) tide effects, but is unlikely to manifest specifically as modeled. Other effects—such as tsunami induced redistribution of sediments and the long-term bathymetric recovery (including the tectonic rebound)—would require morphodynamic modeling (Allan et al., 2018). Furthermore, infrastructure failure would result in morphodynamic feedbacks, especially at the mouth of the Columbia River (Kaminsky et al., 2010) and are not included in this analysis. Post seismic deformation, either by afterslip or viscoelastic deformation (e.g., Suito & Freymueller, 2009), is poorly known for Cascadia ruptures (Walton et al., 2021), but for the M9 Alaska earthquake of 1964, as much as 125 cm of post-seismic uplift affected the Kodiak Island and the Kenai Peninsula over the ensuing 35 years (Huang et al., 2020), indicating the possible magnitude of post-quake rebound for the CSZ.

5. Habitat Succession

The modeled tidal and habitat changes presented here suggests that an M9 event will produce a nearly total habitat disturbance, similar in completeness to other types of

extreme events such as the Mount St. Helens explosion in 1980 (Dale et al., 2005). We anticipate that nearly all floodplain wetland communities would first experience die-off due to frequent inundation after land subsidence and increased tidal range; these results are consistent with the observations of "ghost trees" that died in 1700 and are still found in estuaries of the Pacific Northwest (Atwater, 1987). In the lower estuary, sand deposition on subsided marsh planforms could result in higher marsh elevation than predicted by co-seismic subsidence alone (Rogers, 1996). Nonetheless, our bathymetric and habitat change scenario will likely be modified by both the acute erosion/deposition caused by the tsunami and longer term morphodynamics responses. Additionally, some of the changes in elevational bands are expected to occur in developed regions, particularly downstream of RKM-20 (for instance, the Warrenton airport, Figure 3). It is unknown whether presently developed areas would be abandoned and transition to wetland habitat, or be retained for human use. If retained, much of the developed region would be lower than the 2 year floodplain (which corresponds approximately to the spatial extent of our wetland mapping), and would likely be at risk for persistent high-tide flooding (Thompson et al., 2021) as well as catastrophic inundation during major river floods.

Post CSZ-rupture recovery of estuarine ecosystems will almost certainly take decades to centuries. For example, Benson et al. (2001) found a recovery time of roughly 100 years for Sitka spruce (*Picea sitchensis*) to recolonize sites following the 1700 earthquake. Recent work by Peck et al. (2022) found a 200-year recovery post-CSZ rupture for high marsh at nearby Netarts Bay, Oregon. These recovery rates, however, depend significantly on the balance between relative interseismic SLR and overall sediment supply, which in the LCRE has greatly decreased over the past century (Gelfenbaum et al., 2001; Templeton & Jay, 2013). Moreover, global sea-level rise is accelerating (Nerem et al., 2018), further increasing future vulnerabilities.

6. Conclusions and Broader Impacts

We find that a coseismic rupture can significantly alter the distributions of habitats and tidal ranges in the lower Columbia River Estuary (LCRE) through both land subsidence and subsequent changes to hydrodynamics. Infrastructural failure and floodplain liquefaction may modify these impacts. We find an increase in tidal amplitudes from the mouth of the Columbia River to the confluence of the Willamette River due to deepening as a result of a Cascadia Subduction Zone (CSZ) rupture, and that ~93% of current estuarine habitat will be converted to a lower elevation classification. Because subsidence changes tidal hydrodynamics, the simpler bathtub approach cannot fully reproduce the predicted habitat distributions of the hydrodynamic simulations.

Modeling predicts that a CSZ rupture similar to the last one of CE 1700 would reduce estuarine intertidal habitat by ~4,900 ha, a 24% reduction from current intertidal habitat (20,230 ha) and ~3.3% of the historical 146,800 ha of habitat. The resulting subsidence, liquefaction, and infrastructure damage will also alter the habitat of most of the 2,800 ha of floodplain restored on the Columbia River from 2004 to 2021 (Littles et al., 2022). Recent work outlines a planning framework for wetland restoration throughout the LCRE (Hood et al., 2022) but does not account for likely effects of CSZ ruptures. Developing wetland restoration approaches, land acquisition priorities, and management strategies that accommodate predicted coseismic subsidence are likely required to ensure the long-term viability of restoration efforts (Allan et al., 2018), both in the LCRE and in other subduction zone estuaries. LCRE habitat changes caused by coseismic subsidence are influenced by the steep upland topography surrounding much of the estuary and river, which limits the conversion of uplands into wetland habitat and forces a 29% decrease in intertidal area. The resulting "coastal squeeze," which also occurs within other Eastern Pacific estuaries due to sea-level rise, limits the options for coastal retreat that might be available on a coastal plain and highlights the importance of gaining better estimates of sediment supply and post-event morphological change.

Data Availability Statement

Model outputs from the Delft3D-FM hydrodynamic model needed to recreate the study are archived in the DRYAD data repository (DOI: https://doi.org/10.7280/D1MD7P). The data used in this study are available at the following sources described below. The tidal forcing was developed using the TPXO9-atlas (https://www.tpxo.net/global/tpxo9-atlas). USGS streamflow records are available from https://maps.waterdata.usgs.gov/mapper/index.html by searching by site number, as follows: Cowlitz River #14243000, Lewis River #14220500, Willamette River #14211720, and Sandy River #14142500. U.S. Army Corps of Engineers (U.S. Army Corps of Engineers, 2022) Bonneville Dam releases are available from: https://www.nwd-wc.usace.army.mil/dd/common/projects/www/

bon.html. NOAA Station data are available from: https://tidesandcurrents.noaa.gov https://maps.waterdata.usgs.gov/mapper/index.html by searching by site number, as follows: Cape Disappointment, WA #9440581, Astoria, OR #9439040, Skamokawa, WA #9440569, Wauna, OR #9439099, Longview, WA #9440422, St. Helens, OR #9439201, and Vancouver, WA #9440083. The U.S. Geological Survey National Land Cover Use Database (NLCD, 2019) is found at: https://www.usgs.gov/centers/eros/science/national-land-cover-database. Data from vegetation surveys are available from the following studies: Borde et al. (2011, 2020).

Acknowledgments
We thank the Bonneville Power Administration (BPA project 2002-077-00) and BPA Estuary Lead Jason Karnezis for funding most of this work. Any use of trade, firm, or product names is for descriptive purposes only and does not imply endorsement by the U.S. Government. Modeling was performed using PNNL Institutional Computing at Pacific Northwest National Laboratory. SAT was partially funded by National Science Foundation project 2013280. We acknowledge Tim Carlson of PNNL Institutional Computing for helping set up the Delft3D-FM model used in this study. The authors would like to thank Brian Atwater from the U.S. Geological Survey for organizing the fieldwork to survey liquefaction on the Columbia River. We also thank Kees Nederhoff, Ardi Mortis, and Niels Borsboom from Deltares for their support in developing the Delft3D-FM model. Finally, the authors would like to thank the two anonymous reviewers provided by the journal and additional reviewer from the U.S. Geological Survey, whose comments greatly improved the quality of the manuscript.

References

Al-bahadily, A. (2020). *Long term changes to the lower Columbia River estuary (LCRE) hydrodynamics and salinity patterns*. Dissertation. Portland State University.

Allan, J. C., Zhang, J., O'Brien, F. E., & Gabel, L. L. (2018). *Columbia river tsunami modeling: Toward improved maritime planning response. Special Paper 51*. Oregon Department of Geology and Mineral Industries.

Atwater, B. F. (1987). Evidence for great Holocene earthquakes along the outer coast of Washington State. *Science*, *236*(4804), 942–944. https://doi.org/10.1126/science.236.4804.942

Atwater, B. F., Musumi-Rokkaku, S., Satake, K., Tsuji, Y., & Yamaguchi, D. K. (2011). *The orphan tsunami of 1700—Japanese clues to a parent earthquake in North America. USGS Professional Paper*. University of Washington Press.

Atwater, B. F., & Yamaguchi, D. K. (1991). Sudden, probably coseismic submergence of Holocene trees and grass in coastal Washington State. *Geology*, *19*(7), 706–709. https://doi.org/10.1130/0091-7613(1991)019<0706:spcsoh>2.3.co;2

Baldwin, A. H., Hammerschlag, R. S., & Cahoon, D. R. (2019). Evaluating restored tidal freshwater wetlands. In *Coastal wetlands* (pp. 889–912).

Benson, B. E., Atwater, B. F., Yamaguchi, D. K., Amidon, L. J., Brown, S. L., & Lewis, R. C. (2001). Renewal of tidal forests in Washington State after a subduction earthquake in AD 1700. In *Quaternary research* (pp. 139–147).

Borde, A. B., Diefenderfer, H. L., Zimmerman, S. A., Cullinan, V. I., & Thom, R. M. (2020). Ecohydrology of wetland plant communities along an estuarine to Tidal River gradient. *Ecosphere*, *11*(9). https://doi.org/10.1002/ecs2.3185

Borde, A. B., Zimmerman, S. A., Kaufmann, R. M., Diefenderfer, H. L., Sather, N. K., & Thom, R. M. (2011). Lower Columbia River and estuary restoration reference site study. 2010 final report and site summaries (PNWD-4262). Pacific northwest national lab (PNNL). https://www.osti.gov/biblio/1771189

Burgette, R. J., Weldon, R. J., & Schmidt, D. A. (2009). Interseismic uplift rates for western Oregon and along-strike variation in locking on the Cascadia subduction zone. *Journal of Geophysical Research*, *114*(B1), B01408. https://doi.org/10.1029/2008jb005679

Chen, C., Lindell, M. K., & Wang, H. (2021). Tsunami preparedness and resilience in the Cascadia subduction zone: A multistage model of expected evacuation decisions and mode choice. *International Journal of Disaster Risk Reduction*, *102244*, 102244. https://doi.org/10.1016/j.ijdrr.2021.102244

Dale, V. H., Swanson, F. J., & Crisafulli, C. M. (2005). Disturbance, survival, and succession: Understanding ecological responses to the 1980 eruption of Mount St. Helens. In *Ecological responses to the 1980 eruption of Mount St. Helens* (pp. 3–11).

Eidam, E. F., Sutherland, D. A., Ralston, D. K., Conroy, T., & Dye, B. (2021). Shifting sediment dynamics in the Coos Bay Estuary in response to 150 years of modification. *Journal of Geophysical Research: Oceans*, *126*(1), e2020JC016771. https://doi.org/10.1029/2020jc016771

Gelfenbaum, G., Buijsman, M. C., Sherwood, C. R., Moritz, H. R., & Gibbs, A. E. (2001). Coastal evolution and sediment budget at the mouth of the Columbia River. In *Coastal dynamics* (pp. 818–827). American Society of Civil Engineers.

Gerwing, T. G., Davies, M. M., Clements, J., Flores, A. M., Thomson, H. M., Nelson, K. R., et al. (2020). Do you want to breach an embankment? Synthesis of the literature and practical considerations for breaching of tidally influenced causeways and dikes. *Estuarine, Coastal and Shelf Science*, *245*, 107024. https://doi.org/10.1016/j.ecss.2020.107024

Helaire, L. T., Talke, S. A., Jay, D. A., & Mahedy, D. (2019). Historical changes in lower Columbia River and estuary floods: A numerical study. *Journal of Geophysical Research: Oceans*, *124*(11), 7926–7946. https://doi.org/10.1029/2019jc015055

Hood, G. W., Blauvelt, K., Bottom, D. L., Castro, J. M., Johnson, G. E., Jones, K. K., et al. (2022). Using landscape ecology principles to prioritize habitat restoration projects across the Columbia River Estuary. *Restoration Ecology*, *30*(3), e13519. https://doi.org/10.1111/rec.13519

Huang, K., Hu, Y., & Freymueller, J. T. (2020). Decadal viscoelastic postseismic deformation of the 1964 Mw9. 2 Alaska earthquake. *Journal of Geophysical Research: Solid Earth*, *125*(9), e2020JB019649. https://doi.org/10.1029/2020jb019649

Jay, D. A., Borde, A. B., & Diefenderfer, H. L. (2016). Tidal-fluvial and estuarine processes in the lower Columbia River: II. Water level models, floodplain wetland inundation, and system zones. *Estuaries and Coasts*, *39*(5), 1299–1324. https://doi.org/10.1007/s12237-016-0082-4

Jay, D. A., & Naik, P. K. (2011). Distinguishing human and climate influences on hydrological disturbance processes in the Columbia River, USA. *Hydrological Sciences Journal*, *56*(7), 1186–1209. https://doi.org/10.1080/02626667.2011.604324

Kalmbacher, K. D., & Hill, D. F. (2015). Effects of tides and currents on tsunami propagation in large rivers: Columbia River, United States. *Journal of Waterway, Port, Coastal, and Ocean Engineering*, *141*(5), 04014046. https://doi.org/10.1061/(asce)ww.1943-5460.0000290

Kaminsky, G. M., Ruggiero, P., Buijsman, M. C., McCandless, D., & Gelfenbaum, G. (2010). Historical evolution of the Columbia River littoral cell. *Marine Geology*, *273*(1–4), 96–126. https://doi.org/10.1016/j.margeo.2010.02.006

Littles, C., Karnezis, J., Blauvelt, K., Creason, A., Diefenderfer, H., Johnson, G., et al. (2022). Adaptive management of large-scale ecosystem restoration: Increasing certainty of habitat outcomes in the Columbia River Estuary, USA. *Restoration Ecology*, *30*(8), e13634. https://doi.org/10.1111/rec.13634

Madin, I. P., & Burns, W. J. (2012). *Ground motion, ground deformation, tsunami inundation, coseismic subsidence, and damage potential maps for the 2012 Oregon Resilience Plan for Cascadia Subduction Zone Earthquakes*. Open File Report O-13-06. State of Oregon Department of Geology and Mineral Industries.

Marcoe, K., & Pilson, S. (2017). Habitat change in the lower Columbia River estuary. *Journal of Coastal Conservation*, *21*(4), 505–525. https://doi.org/10.1007/s11852-017-0523-7

Monserud, R. A., & Leemans, R. (1992). Comparing global vegetation maps with the Kappa statistic. *Ecological Modelling*, *62*(4), 275–293. https://doi.org/10.1016/0304-3800(92)90003-w

Naiman, R. J., Alldredge, J. R., Beauchamp, D. A., Bisson, P. A., Congleton, J., Henny, C. J., et al. (2012). Developing a broader scientific foundation for river restoration: Columbia River food webs. *Proceedings of the National Academy of Sciences*, *109*(52), 21201–21207. https://doi.org/10.1073/pnas.1213408109

Nasseri, A., Turel, M., Yin, Y., & Lai, T. (2014). Study of the impact of a magnitude 9.0 Cascadia subduction zone earthquake on British Columbia, Canada. In *Tenth US national conference on earthquake engineering*.

National Land Cover Database. (2019). Retrieved from https://www.usgs.gov/centers/eros/science/national-land-cover-database?qt-science_center_objects=0#qt-science_center_objects

Nederhoff, K., Saleh, R., Tehranirad, B., Herdman, L., Erikson, L., Barnard, P. L., & Van der Wegen, M. (2021). Drivers of extreme water levels in a large, urban, high-energy coastal estuary–A case study of the San Francisco Bay. *Coastal Engineering*, *170*, 103984. https://doi.org/10.1016/j.coastaleng.2021.103984

Nelson, A. R., Atwater, B. F., Bobrowsky, P. T., Bradley, L. A., Clague, J. J., Carver, G. A., et al. (1995). Radiocarbon evidence for extensive plate-boundary rupture about 300 years ago at the Cascadia subduction zone. *Nature*, *378*(6555), 371–374. https://doi.org/10.1038/378371a0

Nerem, R. S., Beckley, B. D., Fasullo, J. T., Hamlington, B. D., Masters, D., & Mitchum, G. T. (2018). Climate-change–driven accelerated sea-level rise detected in the altimeter era. *Proceedings of the National Academy of Sciences of the United States of America*, *115*(9), 2022–2025. https://doi.org/10.1073/pnas.1717312115

NLCD. (2019). *National land cover database*. United States Geological Survey. Retrieved from https://www.usgs.gov/centers/eros/science/national-land-cover-database

NOAA. (2022). Tides and currents. Retrieved from https://tidesandcurrents.noaa.gov/

O'Connor, J. E., Wells, R. E., Bennett, S. E., Cannon, C. M., Staisch, L. M., Anderson, J. L., et al. (2021). Arc versus river—The geology of the Columbia River gorge.

Peck, E. K., Guilderson, T. P., Walczak, M. H., & Wheatcroft, R. A. (2022). Recovery rate of a salt marsh from the 1700 CE Cascadia Subduction Zone earthquake. *Geophysical Research Letters*, *49*, e2022GL099115. https://doi.org/10.1029/2022GL099115

Rogers, A. M. (1996). *Assessing earthquake hazards and reducing risk in the Pacific Northwest* (Vol. 1). Government Report, U.S. Government Printing Office.

Suito, H., & Freymueller, J. T. (2009). A viscoelastic and afterslip postseismic deformation model for the 1964 Alaska earthquake. *Journal of Geophysical Research*, *114*(B11), B11404. https://doi.org/10.1029/2008jb005954

Symonds, A. M., Vijverberg, T., Post, S., Van Der Spek, B. J., Henrotte, J., & Sokolewicz, M. (2016). Comparison between Mike 21 FM, Delft3D and Delft3D FM flow models of western port bay, Australia. *Coastal Engineering*, 1–12.

Takabatake, T., St-Germain, P., Nistor, I., Stolle, J., & Shibayama, T. (2019). Numerical modelling of coastal inundation from Cascadia Subduction Zone tsunamis and implications for coastal communities on western Vancouver Island, Canada. *Natural Hazards*, *98*(1), 267–291. https://doi.org/10.1007/s11069-019-03614-3

Talke, S. A., & Jay, D. A. (2020). Changing tides: The role of natural and anthropogenic factors. *Annual Review of Marine Science*, *12*(1), 121–151. https://doi.org/10.1146/annurev-marine-010419-010727

Talke, S. A., Mahedy, A., Jay, D. A., Lau, P., Hilley, C., & Hudson, A. (2020). Sea level, tidal, and river flow trends in the lower Columbia River Estuary, 1853–present. *Journal of Geophysical Research: Oceans*, *125*(3), e2019JC015656. https://doi.org/10.1029/2019jc015656

Templeton, W. J., & Jay, D. A. (2013). Lower Columbia River sand supply and removal: Estimates of two sand budget components. *Journal of Waterway, Port, Coastal, and Ocean Engineering*, *139*(5), 383–392. https://doi.org/10.1061/(asce)ww.1943-5460.0000188

Thompson, P. R., Widlansky, M. J., Hamlington, B. D., Merrifield, M. A., Marra, J. J., Mitchum, G. T., & Sweet, W. (2021). Rapid increases and extreme months in projections of United States high-tide flooding. *Nature Climate Change*, *11*(7), 584–590. https://doi.org/10.1038/s41558-021-01077-8

Tolkova, E., Tanaka, H., & Roh, M. (2015). Tsunami observations in rivers from a perspective of tsunami interaction with tide and riverine flow. *Pure and Applied Geophysics*, *172*(3–4), 953–968. https://doi.org/10.1007/s00024-014-1017-2

U.S. Army Corps of Engineers. (2022). Bonneville dam and lake. Retrieved from https://www.nwd-wc.usace.army.mil/dd/common/projects/www/bon.html

Walton, M. A., Staisch, L. M., Dura, T., Pearl, J. K., Sherrod, B., Gomberg, J., et al. (2021). Toward an integrative geological and geophysical view of Cascadia subduction zone earthquakes. *Annual Review of Earth and Planetary Sciences*, *49*(1), 367–398. https://doi.org/10.1146/annurev-earth-071620-065605

Yamaguchi, D. K., Atwater, B. F., Bunker, D. E., Benson, B. E., & Reid, M. S. (1997). Tree-ring dating the 1700 Cascadia earthquake. *Nature*, *389*(6654), 922–923. https://doi.org/10.1038/40048

Yeh, H., Tolkova, E., Jay, D. A., Talke, S. A., & Fritz, H. (2012). *Tsunami hydrodynamics in the Columbia River*. Portland State University Dissertation.

References From the Supporting Information

Atwater, B. F. (1994). *Geology of holocene liquefaction features along the lower Columbia River. Open-file report 94-209*. U.S. Geological Survey.

Atwater, B. F. (2020). *Data compiled from stratigraphic and tree-ring studies of late Holocene earthquakes and tsunamis at Copalis river, Grays Harbor, Willapa Bay, and Columbia River, Washington and Oregon. Survey data release*. U.S. Geological Survey.

Atwater, B. F., & Hemphill-Haley, E. (1997). *Recurrence intervals for great earthquakes of the past 3500 years of northeastern Willapa Bay. Professional Paper*. U.S. Geological Survey.

Cohen, J. (1960). A coefficient of agreement for nominal scales. *Educational and Psychological Measurement*, *20*(1), 37–46. https://doi.org/10.1177/001316446002000104

Egbert, G. D., & Erofeeva, S. Y. (2002). Efficient inverse modeling of Barotropic Ocean tides. *Journal of Atmospheric and Oceanic Technology*, *19*(2), 183–204. https://doi.org/10.1175/1520-0426(2002)019<0183:eimobo>2.0.co;2

Giese, B. S., & Jay, D. A. (1989). Modeling tidal energetics of the Columbia River Estuary. *Estuarine, Coastal and Shelf Science*, *29*(6), 549–571. https://doi.org/10.1016/0272-7714(89)90010-3

Goldfinger, C., Nelson, C. H., Morey, A. E., Johnson, J. E., Patton, J. R., Karabanov, E. B., et al. (2012). *Turbidite event history—Methods and implications for Holocene paleoseismicity of the Cascadia subduction zone. No. 1661-F, U.S.*. Geological Survey.

Harris Geospatial Solutions. (2022). Calculate confusion matrices. Software manual, Broomfield, CO: L3Harris geospatial. Retrieved from https://www.l3harrisgeospatial.com/docs/calculatingconfusionmatrices.html#:~:text=The%20kappa%20coefficient%20measures%20the,of%200%20represents%20no%20agreement

Jay, D. A., Leffler, K., Diefenderfer, H. L., & Borde, A. B. (2015). Tidal-fluvial and estuarine processes in the lower Columbia River: I. Along-channel water level variations, Pacific Ocean to Bonneville Dam. *Estuaries and Coasts*, *38*(2), 415–433. https://doi.org/10.1007/s12237-014-9819-0

Karna, T., & Baptista, A. M. (2016). Evaluation of a long-term hindcast simulation for the Columbia River Estuary. *Ocean Modelling*, *99*, 1–14. https://doi.org/10.1016/j.ocemod.2015.12.007

Kay, D. J., & Jay, D. A. (2003). Interfacial mixing in a highly-stratified estuary. 2. A 'method of constrained differences' approach for the determination of the momentum and mass balances and the energy of mixing. *Journal of Geophysical Research*, *108*(C3), 3073. https://doi.org/10.1029/2002.JC000253

Naik, P., & Jay, D. A. (2011). Distinguishing human and climate impacts on Columbia River: Changes in mean flow and sediment transport. *Journal of Hydrology*, *404*(3–4), 259–277. https://doi.org/10.1016/j.jhydrol.2011.04.035

National Atmospheric and Oceanic Administration. (2022). Tides and currents: Tidal datums. Retrieved from https://tidesandcurrents.noaa.gov/datum_options.html

Nelson, A. R., DuRoss, C. B., Witter, R. C., Kelsey, H. M., Engelhart, S. E., Mahan, S. A., et al. (2021). A maximum rupture model for the central and southern Cascadia subduction zone—Reassessing ages for coastal evidence of megathrust earthquakes and tsunamis. *Quaternary Science Reviews*, *261*, 106922. https://doi.org/10.1016/j.quascirev.2021.106922

Parker, B., Hess, K. W., Milbert, D. G., & Gill, S. (2003). *National Vdatum - the implementation of a national vertical datum transformation database*. U. S. Hydrographic Conference. Biloxi.

Pawlowicz, R., Beardsley, B., & Lentz, S. (2002). Classical tidal harmonic analysis including error estimates in MATLAB using T_TIDE. *Computers & Geosciences*, *28*(8), 929–937. https://doi.org/10.1016/s0098-3004(02)00013-4

Ramsey, C. B. (2009). Bayesian analysis of radiocarbon dates. *Radiocarbon*, *51*(1), 337–360. https://doi.org/10.1017/s0033822200033865

Reimer, P. J., Austin, W. E., Bard, E., Bayliss, A., Blackwell, P. G., Ramsey, C. B., et al. (2020). The IntCal20 Northern Hemisphere radiocarbon age calibration curve (0–55 cal kBP). *Radiocarbon*, *62*(4), 725–757. https://doi.org/10.1017/rdc.2020.41

Stevens, A. W., van der SteegWherry, S. S. A., & Wood, T. M. (2021). Hydrodynamic model of the lower Columbia River, Washington and Oregon, 2017-2020 [Dataset]. U.S. Geological Survey. https://doi.org/10.5066/P9ESBJQ0

U.S. Geological Survey. (2022). *Water data for the nation*. U.S. Geological Survey. https://doi.org/10.5066/F7P55KJN. Retrieved from https://waterdata.usgs.gov/nwis

U.S. Army Corps of Engineers. (2010). *Lower Columbia digital terrain data*. Lower Columbia Estuary Partnership Retrieved from https://www.estuarypartnership.org/our-work/monitoring/habitat-mapping/lower-columbia-digital-terrain-model

U.S. Army Corps of Engineers. (2011). *Structural and Hydraulic analysis of Columbia River pile dikes*. U.S. Army Corps of Engineers Digital Library. Retrieved from https://usace.contentdm.oclc.org/digital/collection/p266001coll1/id/2343/

U.S. Army Corps of Engineers. (2022). National levee database. Retrieved from https://levees.sec.usace.army.mil

van Vliet, J., Bregt, A. K., & Hagen-Zanker, A. (2011). Revisiting Kappa to account for change in the accuracy assessment of land-use change models. *Ecological Modelling*, *222*(8), 1367–1375. https://doi.org/10.1016/j.ecolmodel.2011.01.017

Wherry, S. A., Wood, T. M., Moritz, H. R., & Duffy, K. B. (2018). *assessment of Columbia and Willamette River flood stage on the Columbia corridor levee system at Portland, Oregon, in a future climate. Scientific investigations report 2018-5161*. U.S. Geological Survey.